NEUROSCIENCE
RESEARCH ARTICLE
A. Salamatina et al. / Neuroscience 450 (2020) 81–95

Differential Loss of Spinal Interneurons in a Mouse Model of ALS

Alina Salamatina,[a] Jerry H. Yang,[a] Susan Brenner-Morton,[b] Jay B. Bikoff,[c] Linjing Fang,[d] Christopher R. Kintner,[a] Thomas M. Jessell[b] and Lora B. Sweeney[a]*

[a] *Molecular Neurobiology Laboratory, Salk Institute for Biological Studies, La Jolla, CA 92037, USA*

[b] *Howard Hughes Medical Institute, Zuckerman Institute, Depts. of Neuroscience, and Biochemistry and Molecular Biophysics, Columbia University, New York, NY 10032, USA*

[c] *Department of Developmental Neurobiology, St. Jude Children's Research Hospital, Memphis, TN 38105, USA*

[d] *Waitt Advanced Biophotonics Core, Salk Institute for Biological Studies, La Jolla, CA 92037, USA*

Abstract—Amyotrophic lateral sclerosis (ALS) leads to a loss of specific motor neuron populations in the spinal cord and cortex. Emerging evidence suggests that interneurons may also be affected, but a detailed characterization of interneuron loss and its potential impacts on motor neuron loss and disease progression is lacking. To examine this issue, the fate of V1 inhibitory neurons during ALS was assessed in the ventral spinal cord using the SOD^{G93A} mouse model. The V1 population makes up ~30% of all ventral inhibitory neurons, ~50% of direct inhibitory synaptic contacts onto motor neuron cell bodies, and is thought to play a key role in modulating motor output, in part through recurrent and reciprocal inhibitory circuits. We find that approximately half of V1 inhibitory neurons are lost in SOD^{G93A} mice at late disease stages, but that this loss is delayed relative to the loss of motor neurons and V2a excitatory neurons. We further identify V1 subpopulations based on transcription factor expression that are differentially susceptible to degeneration in SOD^{G93A} mice. At an early disease stage, we show that V1 synaptic contacts with motor neuron cell bodies increase, suggesting an upregulation of inhibition before V1 neurons are lost in substantial numbers. These data support a model in which progressive changes in V1 synaptic contacts early in disease, and in select V1 subpopulations at later stages, represent a compensatory upregulation and then deleterious breakdown of specific interneuron circuits within the spinal cord.

This article is part of a Special Issue entitled: A Commemoration of Thomas M. Jessell's Contributions to Neuroscience.

Key words: amyotrophic lateral sclerosis, spinal cord, inhibitory interneuron, V1 interneuron, motor neuron, differential susceptibility.

INTRODUCTION

Amyotrophic lateral sclerosis (ALS) is a neurodegenerative disease that is characterized by the adult-onset degeneration of motor neurons in the spinal cord and cortex. As disease progresses, patients suffer from increasingly severe motor deficits and eventual fatal paralysis (Hardiman et al., 2017). While motor neuron loss is a defining characteristic of ALS, the extent to which other components of motor circuitry are similarly affected or undergo compensatory changes remains unclear. A better understanding of the underlying cellular and circuit mechanisms of disease progression may be key in devising new treatments to prevent or slow ALS pathology.

Studies of the genetics underlying ALS have revealed that ALS-associated genes span many functional classes but together fail to reveal a common underlying mechanism of disease, suggesting that ALS is a syndrome with a complex etiology involving multiple pathways (Al-Chalabi and Hardiman, 2013). The first-identified ALS-associated gene, superoxide dismutase 1 (SOD1), has nonetheless been a focus of study, as mutations in this gene are associated with both familial (~20%) and sporadic (~5%) disease (Kaur et al., 2016). Transgenic mice expressing multiple copies of the SOD G93A mutant allele (hereafter referred to as SOD^{G93A} mice) phenocopy many of the neurological symptoms and cellular pathology seen in ALS patients, making this mouse line a valuable model to study ALS onset and progression (Lutz, 2018). This progression has been defined by clinical score (CS, Solomon et al., 2011): an early stage (CS1–2; postnatal days 85–110), when SOD^{G93A} mice first exhibit shaking and splaying of the limbs followed by deficits in stride and gait; a mid-stage (CS3–4; postnatal days 110–130), when

*Corresponding author. Address: Institute of Science and Technology Austria, Klosterneuburg, Austria.
E-mail address: lora.sweeney@ist.ac.at (L. B. Sweeney).
Abbreviations: ALS, amyotrophic lateral sclerosis; CS, clinical score; SOD1, superoxide dismutase 1.

https://doi.org/10.1016/j.neuroscience.2020.08.011
0306-4522/

paralysis in one and then both hindlimbs occurs; and a late stage (CS5; postnatal days 130–145), when quadriplegia and death typically occur (Gurney et al., 1994).

This progressive loss of motor function in ALS is accompanied by a prominent but selective loss of motor neurons, a feature that has historically defined the disease. In SOD^{G93A} mice, this loss becomes more severe with time, with a 30% reduction in motor neuron number by early and a 70% reduction by late stages of disease (Chiu et al., 1995). Even at pre-symptomatic stages, motor neurons exhibit changes in electrical properties and synaptic transmission, disrupted axon transport, and cellular stress and caspase activation (reviewed in van Zundert et al., 2012). The prominent loss of motor neurons in both human and mouse models of ALS (Kanning et al., 2010), however, is selective, with certain motor neurons subtypes showing a marked susceptibility and others not. Alpha motor neurons, which drive skeletal muscle contraction, are lost in high numbers over the course of disease, while gamma motor neurons, which innervate muscle spindles and modulate muscle sensitivity, do not decrease in number, even at late stages of disease (Kaplan et al., 2014; Lalancette-Hébert et al., 2016; Morisaki et al., 2016). Moreover, alpha motor neurons themselves exhibit differences in susceptibility to degeneration, with the fast-fatigue subtype the most susceptible, the fast-fatigue-resistant subtype less so, and the slow subtype the least susceptible (Frey et al., 2000; Fischer et al., 2004; Pun et al., 2006). The underlying cause of these differences in susceptibility is not known but could be due to differences in the intrinsic physiology or connectivity of motor neuron subtypes.

While motor neuron pathology is thought to make a large contribution to ALS disease onset, dysfunction of other spinal neurons is likely to contribute to disease progression. In human ALS patients, spinal interneurons, defined cytologically, are lost in significant numbers (Stephens et al., 2006), while in ALS mouse models, interneuron losses have begun to be mapped to defined subsets (van Zundert et al., 2012; Brownstone and Lancelin, 2018). In SOD^{G93A} mice, inhibitory neurons, identified broadly by the expression of the neurotransmitters, GlyT2 and Gad67, upregulate pathological markers of stress and downregulate neurotransmitter expression, (Hossaini et al., 2011). Renshaw cells, a small subpopulation of inhibitory neurons that participate in direct recurrent inhibition of motor neurons, first increase their synaptic contacts onto motor neurons in a proposed compensatory manner and then themselves decrease in number at very late disease stages (Wootz et al., 2013). Excitatory neurons also show a marked decrease in numbers in SOD^{G93A} mice, with loss of the V2a population matching both the extent and timing of motor neuron loss (Romer et al., 2017). Finally, synapses derived from the cholinergic V0c population are found first to be enlarged and then lost during disease progression (Chang and Martin, 2009; Pullen and Athanasiou, 2009; Herron and Miles, 2012), with functional inactivation of this subpopulation in ALS mice affecting motor performance (Landoni et al., 2019; Konsolaki et al., submitted). These lines of evidence increasingly point to a disruption of interneuron circuits in ALS progression, and raise the question of what the mechanistic relationship is between motor neuron loss, interneuron loss and disease stage.

To address this question, a more detailed understanding is needed of how the different classes of spinal interneurons are affected during ALS. Accordingly, we focused on the ventral V1 inhibitory class of neurons, which are derived from a common progenitor domain that gives rise to ~30% of all the ventral inhibitory neurons in the spinal cord, and comprise ~50% of the total inhibitory synaptic contacts onto motor neurons (Zhang et al., 2014). This V1 class includes the well-studied Ia- inhibitory (~13% of total V1) and Renshaw cell (~9% of total V1) subpopulations (Alvarez et al., 2005), which coordinate antagonistic muscle pairs and mediate recurrent inhibition, respectively (Gosgnach et al., 2017). In addition, V1 interneurons can be further parsed molecularly into distinct subpopulations based on combinatorial transcription factor expression (Bikoff et al., 2016; Gabitto et al., 2016; Sweeney et al., 2018). This recent analysis suggests that the V1 population at all spinal cord levels can be assigned to four groups, termed clades, with emerging evidence of clade-specific expression, connectivity and functional properties. Each clade can be further subdivided into multiple subtypes based on their unique expression of different combination of transcription factors, raising the possibility these represent diverse functional subtypes required for motor output at each spinal cord level (Francius et al., 2013; Bikoff et al., 2016; Gabitto et al., 2016; Sweeney et al., 2018). We reasoned that this diversity makes the V1 population an ideal class to examine whether interneuron subtypes are differentially susceptible to ALS progression. Conversely, since the significance of V1 genetic diversity has yet to be fully explored, such analysis of V1 subsets in the context of ALS provides an opportunity to test whether these represent different functional populations.

We assess the number of V1 inhibitory neurons in control and SOD^{G93A} mice during disease progression, using a genetic tracer. At late stages of disease, we find that 40% of V1 inhibitory neurons on average are lost in SOD^{G93A} mice, compared with an approximately 60% loss of motor neurons, 60% loss of V2a excitatory neurons, and limited or no loss of other ventral, $NeuN^{+}$ neurons. This result supports a preferential loss of V1 and V2a compared with other V0, V2b and V3 ventral classes of interneurons. At early stages of disease, we find that V1 inhibitory neurons are less affected than motor and V2a excitatory neurons, demonstrating that V1 loss is a later feature of disease. We further find that V1 inhibitory neurons fall into ALS- susceptible or resistant subpopulations, analogous to the differential susceptibility of motor neuron subtypes. Finally, at early stages of disease before V1 inhibitory neurons are lost in large numbers, we show that V1 synaptic contacts increase on ventral motor neuron cell bodies undergoing stress and death. This increase is consistent with but exceeds that previously observed for Renshaw cells (Wootz et al., 2013). Together these results reveal a generalized early increase in V1 to motor neuron synaptic contacts, and a subsequent selective loss of V1 subpop-

ulations. Such alterations in V1 circuits may point to a broader role of interneurons in modulating the progression and severity of ALS.

EXPERIMENTAL PROCEDURES

Animals

All experiments and procedures were performed according to NIH guidelines and approved by the Institutional Animal Care and Use Committee of the Salk Institute for Biological Studies. The following previously published mouse strains were used in this study: *B6SJL-Tg(SOD1*G93A)1Gur/J*, SOD^{G93A} (Gurney et al., 1994), *En1::Cre* (Sapir et al., 2004), and *B6.Cg-Gt(ROSA)26Sortm14(CAG-tdTomato)Hze/J* (otherwise known as Ai14; Madisen et al., 2010). Genotyping was performed using ExTaq DNA Polymerase (Takara, RR001C) and manufacturer's recommended PCR conditions with the following primers and annealing temperatures: SOD^{G93A} offspring with primers oIMR113 and oIMR114 (Jackson Laboratory, Bar Harbor, MI, USA) at an annealing temperature of 60 °C, En1::Cre offsping with Cre 1 (5′-CCGGTGAACGTGCAAAA CAGGCTCTA-3′) and Cre 2 (5′-CTTCCAGGGCGC GAGTTGATAGC-3′) primers at an annealing temperature of 59 °C, and Ai14 offspring with a combination of Rosa 4 (5′-TCAATGGGCGGGGGTCGTT-3′), 10 (5′-CTCTGCT GCCTCCTGGCTTCT-3′), and 11 (5′-CGAGGCGGATCA CAAGCAATA-3′) primers at an annealing temperature of 66 °C. Age- and gender-matched control or SOD^{G93A} littermates expressing *En1::Cre* and Ai14 were used for analysis. Animals were sacrificed at early (clinical score 1–2, CS1-2; abnormal splay of the hindlimbs and tremors when lifted by the tail; average age = 110 ± 4 days) or late (clinical score 5, CS5; significant paralysis such that they are unable to right themselves after 30 seconds; average age = 124 ± 7 days) disease stages, in accordance with standardized phenotyping criteria defined in Solomon et al., 2011. Control and experimental mice were maintained on a congenic B6SJLF1/J background. Near equal numbers of female and male mice were analyzed for all experiments and were maintained using standard husbandry and housing conditions.

Immunohistochemistry

Mice were anesthetized and subsequently perfused with 1× PBS and then 4% paraformaldehyde. The spinal cord was then dissected out, post-fixed in 4% PFA for two hours at 4 °C, washed with 1× PBS, and immersed in 30% sucrose for at least 12 h, until equalized, before being frozen in Tissue-Tek OCT Compound (Sakura). Cryostat sections (25 μm) were washed with 1X PBS with 0.2% Triton (PBT), incubated with 10% donkey serum (Millipore) in PBT for one hour at room temperature, and then primary antibody in PBT plus 10% donkey serum overnight at 4 °C. Sections were then rinsed with PBT, incubated with secondary antibody in PBT plus 10% donkey serum for 30 min at room temperature, washed in PBT, incubated with DAPI, mounted in PVA/DABCO, and coversliped for imaging. Images were obtained on either a LSM 710 or 780 microscope (Zeiss) at a 512 × 512 or greater resolution using a Plan-Aprochromat 20×/0.8 M27 objective (visualization of neurons) or a LSM 880 Rear Port Laser Scanning Confocal with an Airyscan FAST module (visualization of synapses).

Primary antibodies used were as follows: goat anti-Choline Acetyl-Transferase (ChAT, 1:200, Millipore Sigma, #AB144P), guinea pig anti-Chx10 (Hayashi et al., 2018), rabbit anti-NeuN (1:1000, Millipore Sigma, #ABN78), rabbit anti-ATF3 (1:2000, Millipore Sigma, #HPA001562), rabbit anti-cleaved Caspase 3 (cCasp3, 1:150, Cell Signaling Technology, #9661), goat anti-FoxP2 (1: 1000, Santa Cruz Biotechnology N-16, sc-21069), goat anti-Sp8 (1:500, Santa Cruz Biotechnology, C-18, sc-104661), rat anti-Pou6f2 (Jessell Lab, RRID: AB_2665427), rabbit anti-Calbindin D28K (1:2000, Swant, #CB38), rabbit anti-Nr4a2/Nurr1 (1:500; Santa Cruz Biotechnology, M-196, sc-5568), and guinea pig anti-VGAT (1:1000; Synaptic Systems, #131 004). Donkey anti-goat, anti-guinea pig, anti-rabbit, and anti-rat fluorescent-conjugated secondary antibodies (1:500; Green: Alexa Fluor 488; Red: Cy3 or DyLight 549; and Far-red: Cy5, Alexa Fluor 647 or DyLight649) were obtained from Jackson ImmunoResearch and DAPI from Sigma (1:400; D9542).

Quantification of spinal neuron number and spatial distribution

To determine the number and distribution of neurons in the spinal cord, confocal images were imported into Imaris (Bitplane) and spots were assigned to the nucleus of each neuron either manually or using the "Spots" function followed by manual validation. Thresholds were set to exclude non-specific background immunoreactivity. For transcription factor analysis, variations in levels of expression were not taken into consideration, resulting in a determination of "expressed" or "not expressed." Analysis of the spatial position of each cell body, or spot, was performed as previously described (Bikoff et al., 2016; Gabitto et al., 2016). In short, Cartesian coordinates for each neuron were determined in the transverse spinal cord plane with respect to the midpoint of the central canal, defined as position (0,0), and the lateral and ventral-most edge of the gray matter. The compiled data from all hemi-sections analyzed was then morphed onto a standardized hemi-section that reflected the lumbar spinal cord shape at postnatal day zero (distance from central canal to lateral edge was 650 μm and distance from central canal to ventral edge was 400 μm) or postnatal day 120 (distance from central canal to lateral edge was 840 μm and distance from central canal to ventral edge was 570 μm) levels. Spatial contour analysis was performed as previously described (Bikoff et al., 2016). Related MATLAB codes are available at https://github.com/BPHO-Salk/DifferentialLoss_ALS.git.

Analysis of cell body synaptic contacts

The cell bodies of motor neurons and the neurites of V1 inhibitory neurons were labeled with ChAT

immunohistochemistry and *En1::Cre*-driven TdTomato expression, respectively. To determine the number of V1 synaptic contacts with a given motor neuron, a 1560 × 1560 pixel resolution image z-stack image was acquired with a 0.2 μm z-step via an AIRYscan LSM 880 confocal microscope with a Plan-Apochromat 63×/1.4 Oil DIC M27 lens (Zeiss). Seven consecutive sections at the level of the nucleolus were analyzed and on the single, middle section, the number of synaptic contacts with the motor neuron cell body or proximal dendrites per μm of the neuron's circumference were scored according to the following criteria: (1) a TdTomato-positive synaptic enlargement adjacent to the cell body or proximal dendrite that spanned at least 3 consecutive sections and (2) the presence of a contiguous TdTomato-positive V1 neuronal process in one or more sections adjacent to the enlarged synaptic contact. In control experiments (see Fig. S5), VGAT antibody co-labeling was used to validate that such TdTomato-positive enlargements with a contiguous neurite were synaptic contacts. The cell body circumference of a given motor neuron was determined by tracing its perimeter using Imaris measurement points tool.

Quantification and statistical analyses

All statistical analyses are detailed in figure legends and supplementary Table S1. For each littermate control and SOD mouse, parallel sections were collected every 25 μm over an identical rostro-caudal segment of the lumbar (L3–5), thoracic (T4–6) or brachial (C4–6) spinal cord. Individual sections were then imaged at varying but evenly spaced intervals within this segment—with the first image being the most rostral and the last image being the most caudal. For each animal, an average neuron number per section was then calculated from all sections imaged. For a given number of animal pairs (n = animals), these animal averages were then used for all subsequent statistical analyses. Normality was tested across animal pairs with either a Kolgomorov–Smirnov (large n) or a Shapiro–Wilk (small n) test as appropriate. For normally distributed data, significance of differences between animal means were compared with a two-tailed Student's t or one-way ANOVA plus post-hoc Tukey (parametric). For all other non-normal data, a Mann–Whitney or Kruskal–Wallis plus Dunn's (non-parametric) test was performed. All data are represented as the mean ± sem for a given number of animals, unless otherwise noted.

RESULTS

Spinal motor and interneuron loss at late stages of ALS

To examine differential neuron loss in the ventral spinal cord during ALS, we scored V1 inhibitory, V2a excitatory, motor and total neurons in SOD^{G93A} mice (Gurney et al., 1994) at late stages of disease (Figs. 1A and S1A). This late stage timepoint was defined by the inability of SOD^{G93A} mice to right themselves after thirty seconds, the well-established, phenotyping criteria of clinical score 5 (CS5, also referred to as late stage; average age = 124 ± 7 days; (Solomon et al., 2011). V1 inhibitory neurons were genetically marked by *En1::Cre* (Sapir et al., 2004) and the *CAG.lsl.tdTomato* reporter allele (Ai14; Madisen et al., 2010). Other neuronal populations were scored based on antibody reactivity for established markers of cell type identity: V2a excitatory neurons express Chx10 (Ericson et al., 1997; Crone et al., 2008; Hayashi et al., 2018), and motor neurons express ChAT. NeuN expression was used as a rough measure of total neurons, although restricted expression in some classes like motor neurons (see below) can be used to define subtypes.

We focused our analysis on the lumbar L3–L5 spinal cord and analyzed a representative set of spinal cord sections from SOD^{G93A} mice along with their age- and gender- matched littermate controls. As previously shown (Gurney et al., 1994; Chiu et al., 1995), we found that 58% of the lumbar motor neurons were lost at CS5 (Fig. 1B), with both those located in the lateral (61%) and medial (55%) halves of the spinal cord equally affected (Fig. S1B, C). Motor neurons in the lumbar spinal cord have been reported to vary in their susceptibility, with muscle fiber-innervating alpha motor neurons being the most susceptible, and muscle spindle-innervating gamma motor neurons being the least susceptible (Lalancette-Hébert et al., 2016). We similarly found that alpha motor neurons ($ChAT^+$ $NeuN^+$ with a large cell body perimeter) were markedly reduced in SOD^{G93A} mice at CS5, while gamma motor neurons ($ChAT^+$ $NeuN^-$ with a small cell body perimeter) were unaffected (Fig. S1D–F). In addition, and in agreement with Romer et al. (2017), we found that V2a excitatory interneurons were reduced by 57% in SOD^{G93A} compared with control mice (Fig. 1D). Based on the substantial losses of both motor and excitatory neurons, we explored whether inhibitory neurons might be similarly affected in SOD^{G93A} mice at this late disease stage.

Analysis of the number of V1 inhibitory neurons, indelibly marked by *En1::Cre* expression, revealed a 39% reduction in SOD^{G93A} compared to control mice (Fig. 1C). By contrast, no significant difference was detected in the same control and SOD^{G93A} mice in the total number of ventral $NeuN^+$ neurons, after excluding motor and V1 inhibitory neurons and because V2a excitatory neurons comprise a minor component of the total (Fig. 1E). In summary, we find that a significant fraction of V1 inhibitory neurons are lost at late stages of disease, and that this loss in combination with that of motor neurons and V2a excitatory neurons is greater than that of other neurons in the ventral spinal cord.

Spinal motor and interneuron loss at early stages of ALS

Previous studies have demonstrated that inhibitory neurons are unaffected at presymptomatic stages of disease (Hossaini et al., 2011), raising the question of when the V1 losses we observe occur. To explore the progression of subtype-specific neuronal loss in ALS, we examined SOD^{G93A} mice at a symptomatic but early

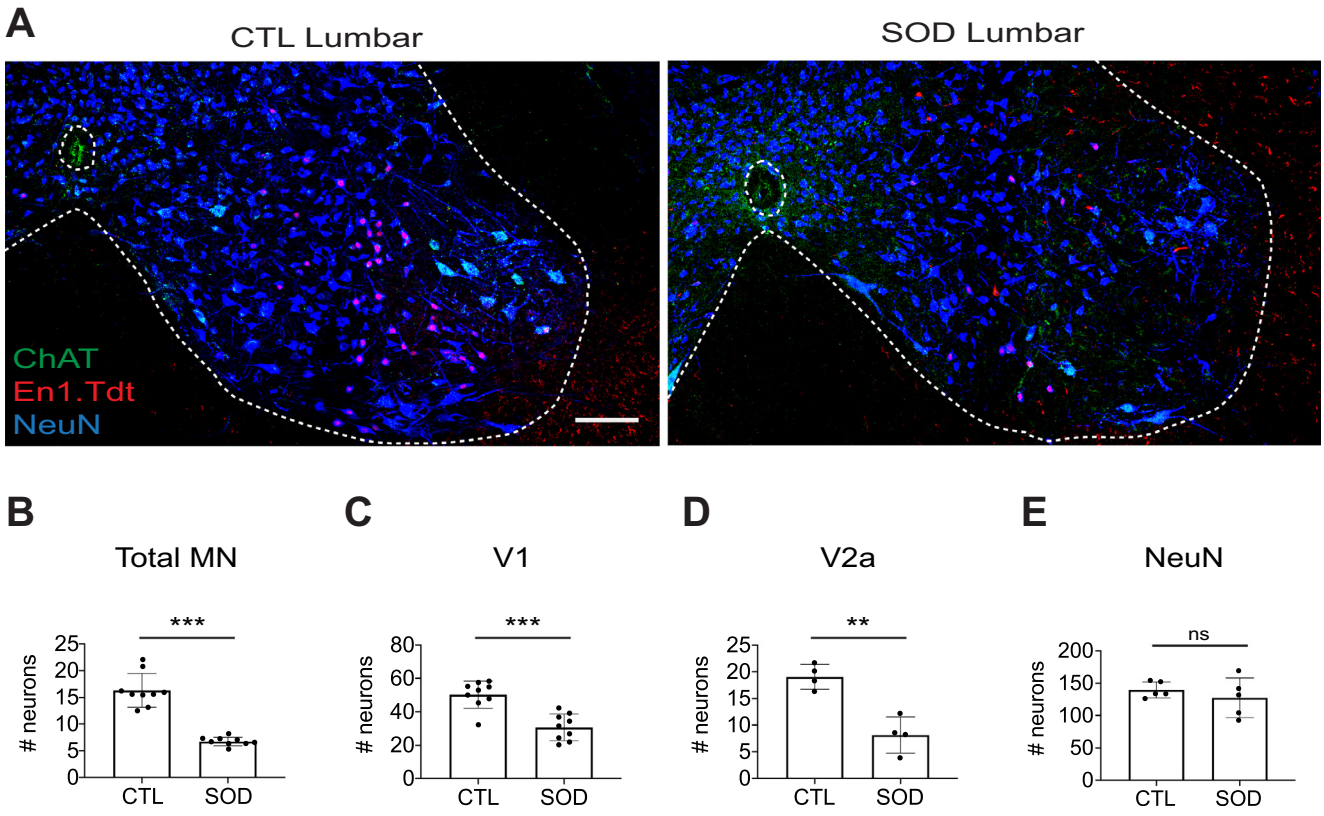

Fig. 1. Neuronal loss at late stages of disease in the SOD^{G93A} mouse model of ALS. **(A)** Hemi-sections of the ventral L3–L5 spinal cord of a control (CTL, left) and a CS5 SOD^{G93A} (SOD, right) mouse were stained for markers of motor (ChAT$^+$, green), V1 inhibitory (En1.TdT$^+$, red), and total NeuN$^+$ neurons (blue). ChAT$^+$NeuN$^+$, cyan. En1.TdT$^+$NeuN$^+$, magenta. Scale bar = 100 μm. **(B–E)** Ventral neuron loss in the lumbar spinal cord of CS5 SOD^{G93A} mice versus littermate controls: motor neurons (**(B)**: $P < 0.0001$, 59% decrease), V1 inhibitory neurons (**(C)**: $P < 0.0001$, 39% decrease), V2a excitatory neurons (**(D)**: $P = 0.0019$, 57% decrease), and ventral NeuN-positive neurons excluding motor and V1 inhibitory neurons (**(E)**: $P = 0.4345$, no decrease). In the scatter dot plots shown here and in subsequent Figures, each point represents the average neuron number per 25 μm lumbar hemi-section based on multiple sections from a given animal, where the number of sections analyzed for each animal is provided in Table S1. The number of points represents the number of SOD^{G93A} and control littermate pairs analyzed. Ventral cell body position was defined as below the midpoint of the central canal. *P* values were determined by a Mann–Whitney **(B)** or an unpaired, two-tailed *t*-test **(C–E)** as appropriate (***$P < 0.001$; **$P < 0.01$; *$P < 0.05$). All subsequent statistical analyses are detailed in Experimental Procedures and Supplementary Table S1.

stage of disease onset, a clinical score of 1–2 (CS1-2, also referred to as early stage; average age = 110 ± 4 days). At this stage, mice display hyperflexion of the hindlimbs when suspended by the tail but no other movement deficits during the locomotor step cycle (Solomon et al., 2011). Previously, it has been found that only the most highly susceptible, alpha fast-fatigue motor neurons, which make up approximately one third of the total, are lost at this stage, while other motor neurons are still present (Lalancette-Hébert et al., 2016). V2a excitatory neurons similarly are less affected at this earlier disease stage in SOD^{G93A} mice, with only a 20% loss in V2a neuron number (Romer et al., 2017). Consistent with these previous results, in the lumbar spinal cord of CS1-2 SOD^{G93A} mice compared to control littermates (Fig. 2-A–D), we found that the number of motor neurons (Fig. 2C) and V2a excitatory neurons (Fig. 2D) are decreased on average by 39% and 29%, respectively.

In contrast, V1 inhibitory neurons were reduced by only 13% at this earlier disease stage (Fig. 2E). To examine the relationship between the differential loss of neuron types within a given animal, we scored V1 inhibitory, V2a excitatory, and motor neuron numbers in adjacent spinal cord sections from pairs of gender- and aged-matched control and SOD^{G93A} littermates. We then plotted these data at early (CS1-2) and late (CS5) stages to compare the proportional magnitude of loss of each neuronal population between animals and over disease progression (Fig. 2F–H and Table S1). Across individual animal pairs and disease stages, motor, V2a and V1 losses were well-correlated, demonstrating a potential relationship between loss of these interconnected neuron types. However, the extent of loss varied with motor and V2a loss occurring in a near one-to-one ratio (Fig. 2F) and consistently greater than V1 loss (Fig. 2G, H).

To examine further whether the pathology of V1 inhibitory neurons is less advanced than motor neurons at early stages, we labeled lumbar sections of CS1–2 SOD^{G93A} mice with antibodies against the cell stress marker, ATF3 (Fig. S2A–C) and the cell death marker, cleaved Caspase 3 (cCasp3; Fig. S2D–F). At late stages of disease, both ATF3 and cCasp3 are detected in motor and interneurons (Li et al., 2000; Pasinelli

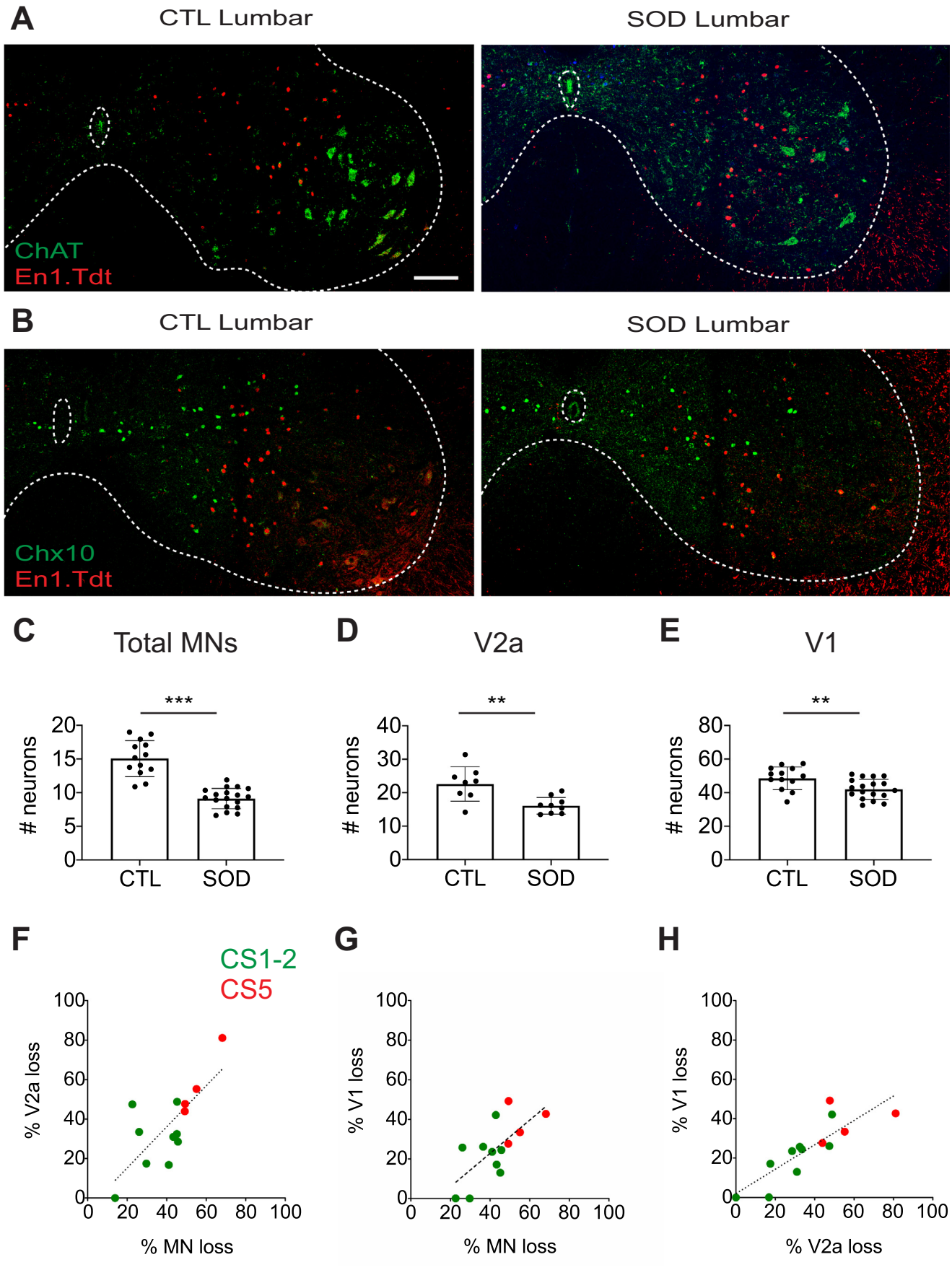
A
CTL Lumbar
SOD Lumbar
ChAT
En1.Tdt
B
CTL Lumbar
SOD Lumbar
Chx10
En1.Tdt
C
Total MNs
***
neurons
CTL
SOD
D
V2a
**
neurons
CTL
SOD
E
V1
**
neurons
CTL
SOD
F
CS1-2
CS5
% V2a loss
% MN loss
G
% V1 loss
% MN loss
H
% V1 loss
% V2a loss

et al., 2000; Hossaini et al., 2011). However, at CS1–2, while motor neurons that express these markers were readily observed, very little expression was detected in V1 inhibitory neurons in the same section, providing additional support that motor neurons are more advanced in their degeneration than V1 inhibitory neurons at this stage. Together these data suggest that a subset of V1 inhibitory interneurons are lost in ALS but that V1 degeneration occurs after that of motor neurons and V2a excitatory neurons.

Clade analysis of inhibitory V1 subtypes in ALS

V1 inhibitory neurons can be subdivided by their physiological and molecular properties, leading to the view that the V1 class is comprised of numerous transcriptionally, anatomically and electrophysiologically diverse subpopulations (Gosgnach et al., 2017). Since only a third of the total V1 population has degenerated in SOD^{G93A} mice even at late stages of disease, we examined whether V1 subpopulations were differentially affected. To address this issue, we first tested whether the transcription factors that subdivide V1 inhibitory neurons at an early postnatal stage also mark similar subpopulations in the adult spinal cord.

We focused our analysis on the four major subgroups of V1 inhibitory neurons, termed clades, which are defined by the mutually exclusive expression of the transcription factors FoxP2, Sp8, Pou6f2, and MafA; include greater than 50% of all V1 inhibitory neurons; and differ in their connectivity and electrophysiological properties (Bikoff et al., 2016; Gabitto et al., 2016). Antibodies against Foxp2, Sp8 and Pou6f2 labeled subsets of V1 inhibitory neurons in the adult (p120–140) (Fig. 3A). MafA staining, which primarily marks Renshaw cells at p0, was not detected in the adult, and thus Calbindin immunoreactivity coupled with ventral cell body position was instead used as a Renshaw cell marker (Benito-Gonzalez and Alvarez, 2012). Strikingly, the percentages of V1 inhibitory neurons (indicating clade size) labeled with these four markers were similar at adult stages (Fig. 3B-–E) to those observed at p0 (Bikoff et al., 2016; Sweeney et al., 2018). Furthermore, at both early postnatal and adult time points, these clade markers showed zero overlap (data not shown), together included more than 50% of all V1 inhibitory neurons, and individually each labeled V1 subpopulations with a spatially-distinct but temporally-conserved settling position (Fig. 3B-–E). Such differences in position between clades but similarities between stages can be most readily observed in the dorsomedial, dorsolateral, and ventral positioning of the $V1^{Sp8}$ (Fig. 3C), $V1^{Pou6f2}$ (Fig. 3D), and $V1^{vCalbindin}$ (Fig. 3E) subpopulations, respectively. These results indicate that transcription factor expression continues to track the V1 clades into adult stages, further supporting that the clade designation is likely to have functional significance for mature V1 interneurons.

Such persistence of transcription factor expression also provides a tool to examine the susceptibility of each clade to degeneration in SOD^{G93A} mice at late CS5 stages of disease. We found that the most dramatic reduction occurred in the $V1^{FoxP2}$ clade (Fig. 3F, 51%), with a smaller but significant reduction in the $V1^{Sp8}$ clade (Fig. 3G, 38%) and no significant change in the $V1^{Pou6f2}$ (Fig. 3H) or $V1^{Calbindin}$ (Fig. 3I) clades. To address the possibility that such differences in susceptibility may in part result from differences in clade size, we performed power analyses. For all clades, we had sufficient power to detect 30% or greater changes in cell number, indicating that undetected changes in $V1^{Pou6f2}$ or $V1^{Calbindin}$ clades are likely to be small or non-existent. These data indicate that V1 loss differs in magnitude between clades, suggesting that V1 inhibitory neurons, like motor neurons, fall into ALS-susceptible and ALS-resistant subpopulations.

Combinatorial analysis of V1 subsets in ALS

Within clades, V1 inhibitory neurons can be further classified into smaller subsets by the combinatorial expression of transcription factors (Bikoff et al., 2016; Gabitto et al., 2016; Sweeney et al., 2018). Like the clades, these smaller subsets may represent functionally distinct subpopulations, rendering them differentially susceptible to ALS. To begin to address this issue, we focused our analysis on the $V1^{FoxP2}$ clade because it is the largest and the most affected, and surveyed the expression of transcription factors that subdivide it at early postnatal stages (Bikoff et al., 2016). We found that Nr4a2 expression was maintained until adult stages, and divided the FoxP2 clade into a Nr4a2-OFF ($V1^{FoxP2+Nr4a2-}$, 75% of the clade) and Nr4a2-ON ($V1^{FoxP2+Nr4a2+}$, 25% of the clade) subpopulation, similar to what has been observed at p0 (Fig. 3J, K),. This similar pattern of Nr4a2 expression at postnatal and adult stages lends support to the functional importance of these transcriptional distinctions within a clade

We further evaluated these clade-derived V1 subsets in ALS at the late CS5 stage of disease. We find in SOD^{G93A} mice that the $V1^{FoxP2+Nr4a2+}$ inhibitory neurons are reduced in number by 78% (Fig. 3N), while

Fig. 2. Lumbar motor and interneuron loss at disease onset. **(A, B)** Hemi-sections of the ventral L3–L5 spinal cord of a control (CTL, left) and a CS1–2 SOD^{G93A} (SOD, right) mouse were stained for markers of either motor (**(A)**: $ChAT^+$, green) or V2a excitatory (**(B)**: $Chx10^+$, green) and V1 inhibitory ($En1.TdT^+$, red) neurons. Scale bar = 100 μm. **(C–E)** Ventral neuron loss in the lumbar spinal cord of CS1–2 SOD^{G93A} mice versus littermate controls: motor neurons (**(C)**: $P < 0.0001$, 40% decrease), V2a excitatory neurons (**(D)**: $P = 0.004$, 29% decrease), and V1 inhibitory neurons (**(E)**: $P = 0.008$, 13% decrease). Scatter dot plots represent average neuron number per 25 μm lumbar hemi-section as described in detail in the legend to Fig. 1. **(F–H)** Animal-by-animal comparisons of motor neuron, V1 inhibitory, and V2a excitatory neuron loss at lumbar levels in CS1–2 (green) and CS5 (red) SOD^{G93A} mice: Motor versus V2a excitatory neurons (F: slope = 1.04; $R^2 = 0.55$), motor versus V1 inhibitory neurons (**(G)**: slope = 0.67; $R^2 = 0.35$), and V2a excitatory versus V1 inhibitory neurons (**(H)** slope = 0.62; $R^2 = 0.70$). Each dot represents the percent decrease in mean SOD vs. CTL neuron number for a single littermate pair (see Table S1 for raw data).

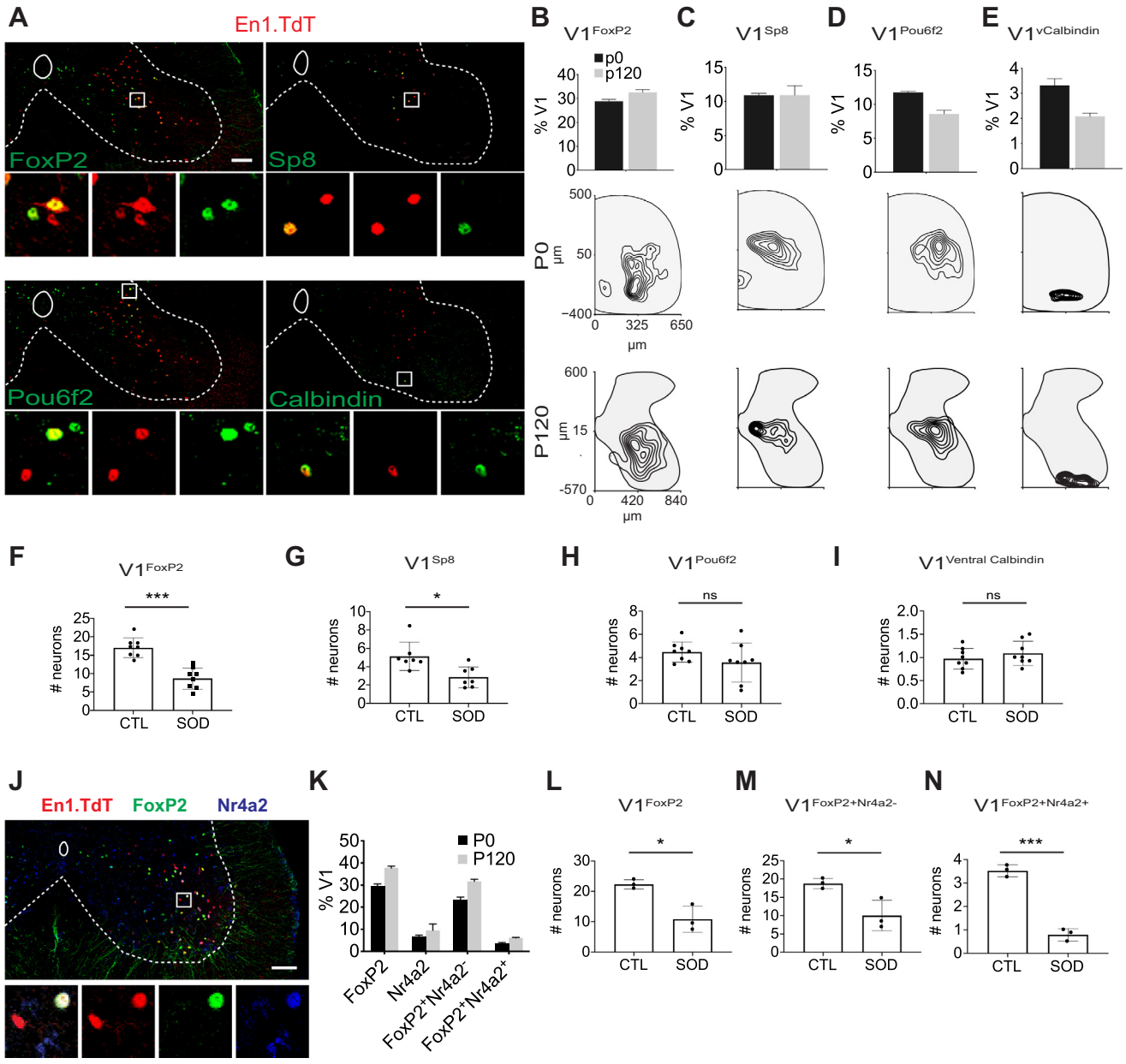

Fig. 3. Differential loss of V1 inhibitory neuron clades in CS5 SOD^{G93A} mice. **(A)** Sections of lumbar level spinal cord from p120 control mice, stained for V1 inhibitory neurons (Red: En1.TdT) and with antibodies (green) against FoxP2, Sp8, Pou6f2 or Calbindin. Panels above show a right hemi-segment, while insets below show overlap and individual channels for a subset of neurons. Scale bar = 100 μm. **(B–E)** V1 clade markers are expressed in similar percentages of V1 inhibitory neurons in early postnatal (P0) and adult (P120) mice. Graphs depict percentage (above), and spatial plots depict position (below), of V1 inhibitory neurons marked by En1.TdT lineage trace and FoxP2 ((**B**), V1^{FoxP2}), Sp8 ((**C**), V1^{Sp8}), Pou6f2 ((**D**), V1^{Pou6f2}) and Calbindin ((**E**), V1^{vCalbindin}) antibodies**.** Spatial plots depict 20th–80th percentile density contours as described in Sweeney et al. (2018) and Experimental Procedures. The Renshaw cell clade is defined as Calbindin-expressing V1 neurons in the ventral-most 20% of the spinal cord. **(F–I)** Quantification of V1 clade susceptibility. V1^{FoxP2} ((**F**): $P < 0.001$, 49% decrease) and V1^{Sp8} ((**G**): $P = 0.0087$, 45% decrease) inhibitory neurons are the most susceptible, while V1^{Pou6f2} ((**H**): $P = 0.1975$) and V1^{vCalbindin} ((**I**): $P = 0.3603$) inhibitory neurons were unaffected at CS5. Scatter dot plots represent average neuron number per 25 μm lumbar hemi-section as described in the legend in Fig. 1. Power analyses based on average and standard deviation measurements indicates 8 animals are sufficient to detect a 30% loss in SOD compared to control animals for all V1 clades. **(J, K)** Nr4a2 transcription factor expression (blue) further subdivides FoxP2-expressing (green) V1 inhibitory neurons (red) into a Nr4a2-on and Nr4a2-off subpopulation at adult stages in control animals **(J)**. Panels above show a right hemi-segment, while insets below show individual channels and overlap for a subset of neurons. These subpopulations are of similar proportions at P0 (black) and adult (P120, gray) stages **(K)**. Scale bar = 100 μm. **(L–N)** Within the V1^{FoxP2} clade, the V1$^{FoxP2+Nr4a2+}$ subpopulation is particularly susceptible at CS5 to neuron loss ((**N**): $P = 0.0002$, 78% decrease), compared with the parental V1^{FoxP2} ((**L**): $P = 0.0120$, 52% decrease) or V1$^{FoxP2+Nr4a2-}$ subpopulation ((**M**): $P = 0.0262$, 47% decrease). Scatter dot plots represent average neuron number per 25 μm lumbar hemi-section as described in the legend of Fig. 1.

total V1^{FoxP2} (Fig. 3L) and V1$^{FoxP2+Nr4a2-}$ neurons (Fig. 3M) are only reduced by half. Thus, a smaller clade-derived subset, like the clades themselves, can vary in their susceptibility, further supporting a model in which specific V1 microcircuits may be differentially lost during disease progression. One implication of this

model is that the $V1^{FoxP2}$ clade is known to contain Ia-inhibitory neurons (Benito-Gonzalez and Alvarez, 2012), suggesting that the dramatic losses we observe for specific FoxP2 subsets might reflect a potential disruption of reciprocal inhibitory circuits in ALS.

Spinal interneuron susceptibility in ALS along the rostro-caudal axis

Variation in motor and inhibitory neuron identity based on physiological and molecular properties is also observed along the rostro-caudal body axis. At limb levels, distinct motor neuron subsets project to flexor–extensor muscles to drive such movements as running and grasping, while at torso-levels, innervate hypaxial and back musculature to control breathing, posture, and the autonomic nervous system (reviewed in Dasen and Jessell, 2009). Similarly, molecularly-distinct V1 subpopulations exist at limb and torso levels with their function as of yet unexplored (Francius et al., 2013; Sweeney et al., 2018). To investigate whether such rostro-caudal differences in motor circuits might confer differential ALS susceptibility, we examined whether and to what extent motor and V1 inhibitory neurons were lost at brachial and thoracic levels of control and SOD^{G93A} mice at the late CS5 stages of disease.

In agreement with previous studies in SOD^{G93A} mice (Chiu et al., 1995), at late CS5 stages of disease, we found that the magnitude of motor neuron loss at different spinal levels varied significantly, with 58% lost at lumbar levels, 41% at brachial levels, and 26% at thoracic levels (Fig. 4A). The decreased susceptibility of thoracic motor neurons can largely be explained by the resistance of the autonomic subpopulation to degeneration (Fig. S3), a finding observed previously in both SOD^{G93A} mice (Chiu et al., 1995) and human ALS patients (Wetts and Vaughn, 1996). Once this motor neuron population is accounted for, somatic motor neurons are equally affected along the entire rostro-caudal axis, with ~50% lost at all spinal cord levels (Figs. 4A, C and S3). In a manner similar to somatic motor neurons, V1 inhibitory neuron loss also occurred to an equal extent along the entire rostro-caudal axis, with an ~40% reduction at all spinal cord levels (Fig. 4B, C). This result may indicate that V1 inhibitory neuron loss is more associated with somatic than with autonomic motor neuron loss.

Given the variation in motor output and circuit identity along the body axis, we evaluated whether V1 subtypes might differ in susceptibility based on rostro-caudal position by refining our analysis to the V1 clades. We found at all spinal cord levels that neurons in the $V1^{FoxP2}$ clade were lost to the same extent (Fig. 4D), and those in the $V1^{Pou6f2}$ and $V1^{vCalbindin}$ clades were largely unaffected (Fig. 4F, G). However, the $V1^{Sp8}$ clade varied in susceptibility by level in SOD^{G93A} mice: at limb levels, $V1^{Sp8}$ neurons decreased in number by ~35%, while at thoracic levels, they did not significantly differ in number (Fig. 4E). These findings support a functional relationship between motor and V1 subsets at different positions along the rostro-caudal axis, with such a relationship potentially underlying differences in ALS circuit susceptibility.

V1 inhibitory – motor neuron synaptic connectivity at early stages of ALS

The results above show that V1 inhibitory neurons are not lost in substantial numbers at early stages of disease, suggesting that an early loss of V1 inhibitory neurons is not an initial cause of motor neuron loss. However, even though V1 neurons are still present, their synaptic contacts onto motor neurons could be disrupted at these earlier stages and lead to motor neuron dysfunction. To examine this possibility, we evaluated the number of V1 synaptic contacts made directly onto the cell body of motor neurons, first in control and then SOD^{G93A} mice.

To provide a baseline for our analysis of SOD^{G93A} mice, we first quantified the total (V1) and Renshaw ($V1^{Calbindin}$) synaptic contacts onto motor neuron cell bodies in control mice. V1 synaptic contacts were scored at ~p110 by counting the number of En1::Cre driven $TdTomato^+/VGAT^+$ boutons on the cell bodies of $ChAT^+$ motor neurons in the lumbar spinal cord (Fig. 5A, B). As shown previously (Alvarez et al., 2005), $ChAT^+$ motor neuron cell bodies at lumbar levels had an average number of 0.07 synapses per micrometer. Nearly every $TdTomato^+$ bouton was $VGAT^+$ (Fig. S4A, B), leading us to score only TdTomato in subsequent experiments. We then further subdivided V1 synaptic contacts onto motor neuron cell bodies based on Calbindin immunoreactivity and dorso-ventral position in the spinal cord. This enabled us to score the number of total (V1), Renshaw ($V1^{Calbindin}$), and non-Renshaw ($V1^{Non\text{-}Calbindin}$) contacts. As shown previously (Carr et al., 1998; Bikoff et al., 2016), we found that Renshaw cells make up only a small portion of total V1 synaptic contacts onto motor neuron cell bodies, and that these $V1^{Calbindin}$ contacts are more numerous on ventral (20% of total V1 contacts) than dorsal motor neurons (5%) (Fig. 5B).

We then determined whether the number of V1 synaptic contacts onto motor neuron cell bodies varied in control and SOD^{G93A} mice. We focused our analysis on the early CS1-2 timepoint, when motor neurons have not yet been lost in dramatic numbers (Fig. 2) but have begun to express markers of stress (10% $ATF3^+$) and cell death (10% $cCasp3^+$) (Fig. S2). To eliminate variation due to cell-to-cell differences in disease state, we restricted our analysis to motor neurons that are actively stressed (Fig. S4C; ATF3-positive) or dying (Fig. S4D; cleaved Casp3-positive) in SOD^{G93A} mice. At these early stages of disease, these stressed or dying motor neurons are likely to be of an alpha fast-fatigue or fast-fatigue resistant subtype(Lalancette-Hébert et al., 2016), and thus, for comparison, we scored the corresponding large sized motor neurons in control animals. We found that the total V1 synaptic contacts onto the cell bodies of stressed or dying motor neurons were similar (dorsal and middle) or increased significantly (ventral) in SOD^{G93A} versus control mice (Fig. 5C). This increase in ventral V1 to motor neuron cell body contacts occurred for both $Calbindin^+$ (Fig. 5D), consistent with previous reports (Wootz et al., 2013), and $Calbindin^-$ V1 synaptic contacts (Fig. 5E), with $Calbindin^-$ synaptic contacts

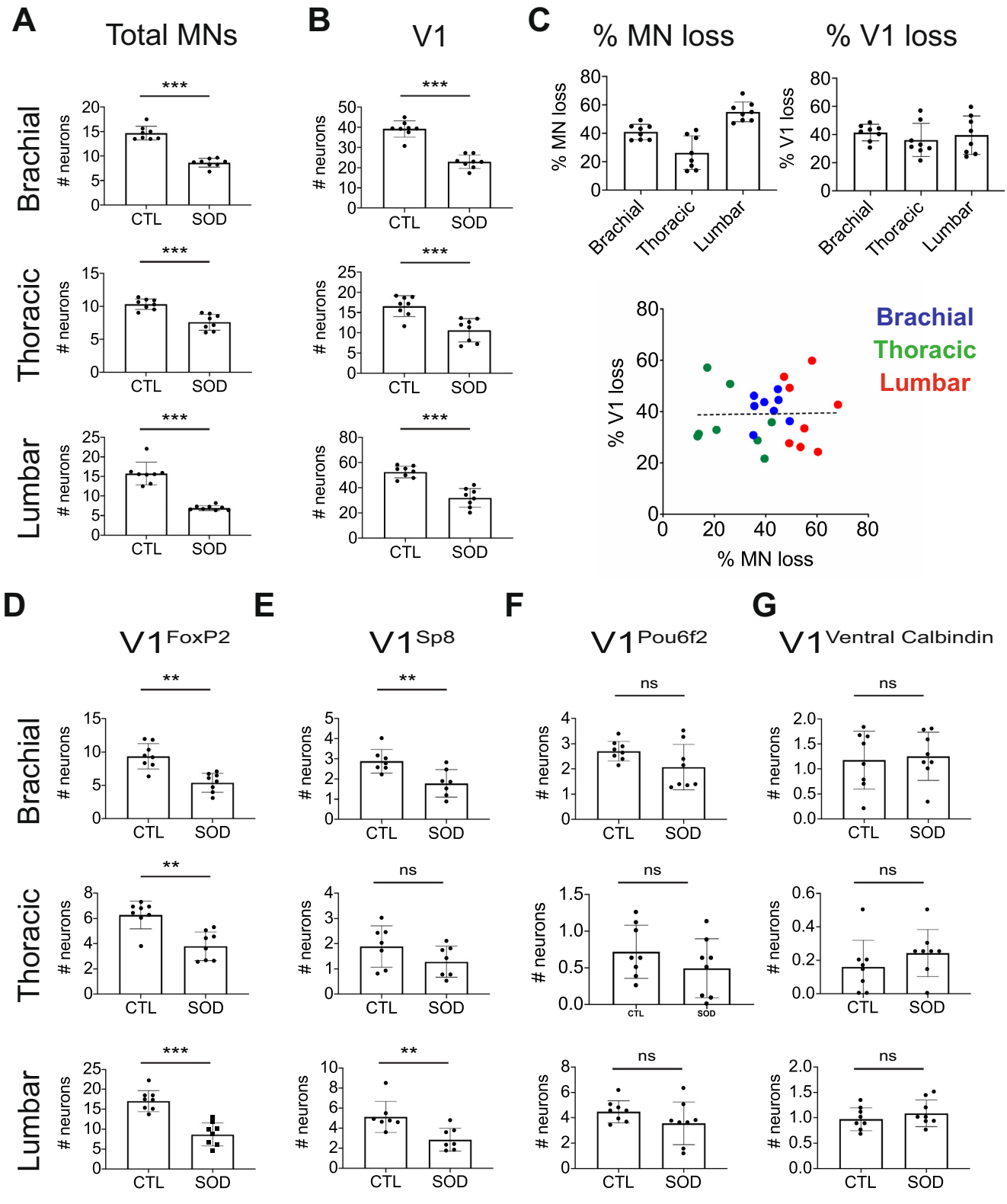
A
Total MNs
B
V1
C
% MN loss
% V1 loss
Brachial
Thoracic
Lumbar
neurons
% MN loss
% V1 loss
CTL
SOD
***
Brachial
Thoracic
Lumbar
D
V1 FoxP2
E
V1 Sp8
F
V1 Pou6f2
G
V1 Ventral Calbindin
**
ns

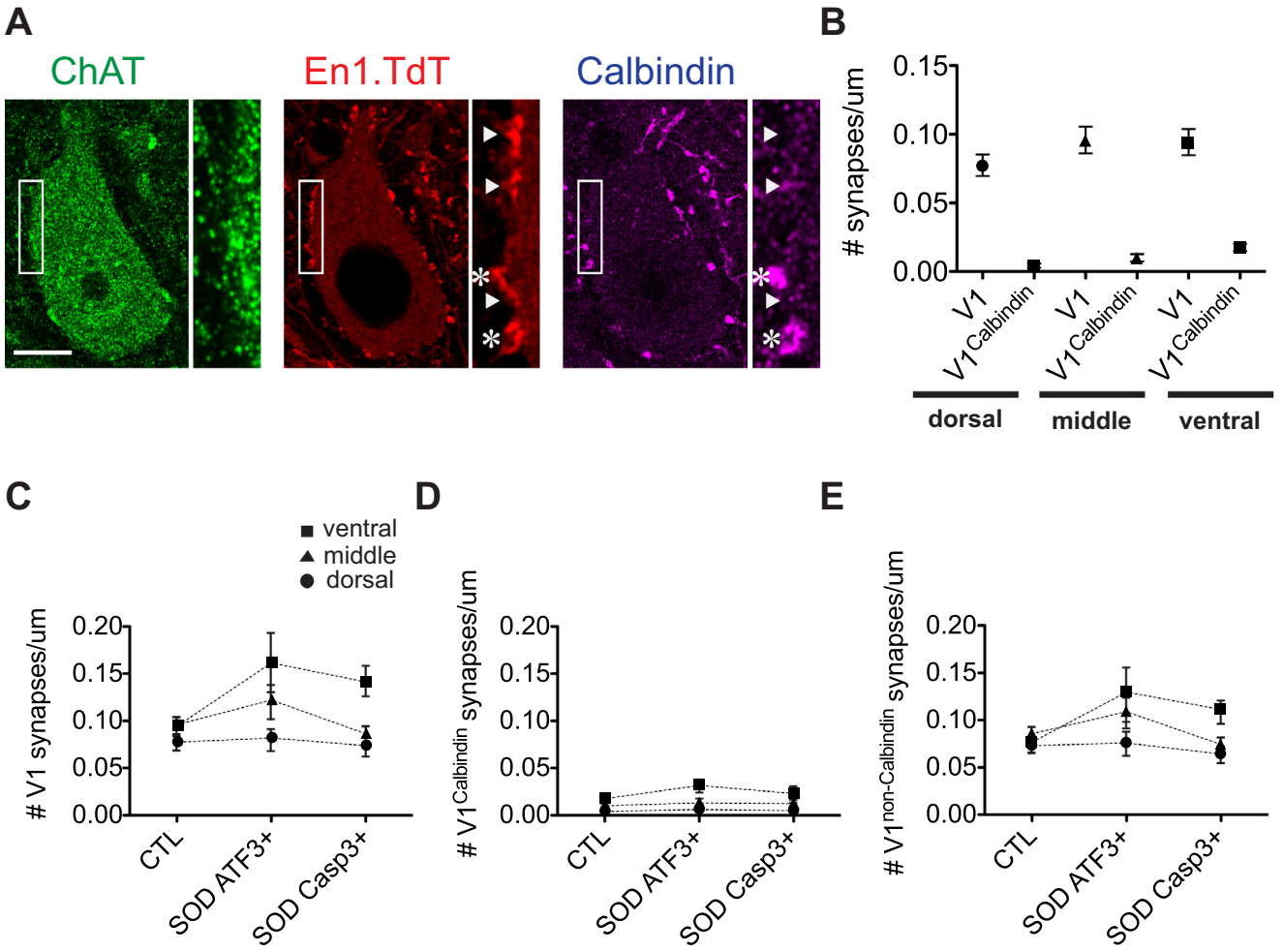

Fig. 5. Analysis of V1 to motor neuron synapses in control and SOD^{G93A} mice at early disease stages. **(A)** Representative images in control mice of lumbar motor neurons (ChAT, green) with V1 synaptic contacts (En1.TdTomato, red) that are either positive (V1^{Calbindin}; asterisk) or negative (V1$^{Non\text{-}Calbindin}$; arrowhead) for Calbindin staining (magenta). Inserts in left panels of a single motor neuron are magnified in the right panel. Scale bar = 10 μm. **(B)** Graphs depict mean ± sem synapse number per micron in control mice of total V1 or V1^{Calbindin} synaptic contacts with ventral, middle or dorsal motor neurons (n = 111 motor neurons in three control adult mice with an average age of ~P110). Data were separated by the ventral (squares), middle (triangles) and dorsal (circles) position of motor neurons within the ventral horn. **(C)** Quantification of V1 synaptic contacts with motor neurons that are stressed (SOD ATF3+; P = 0.0.0087) or dying (SOD cCasp3+; P = 0.0207) in CS1–2 SOD^{G93A} (SOD) versus healthy motor neurons in control (CTL) mice. Data were separated based on motor neuron position as in **(B)**. **(D–E)** Data shown in panel **(C)** are separated out into V1^{Calbindin} **(D)** and V1$^{Non\text{-}Calbindin}$ **(E)** synaptic contacts. In SOD vs CTL mice, V1$^{Non\text{-}Calbindin}$ synaptic contacts are significantly increased on ventral motor neurons that are stressed (P = 0.0186) or dying (P = 0.0259) while V1^{Calbindin} synaptic contacts are significantly increased only on ventral motor neurons that are stressed (P = 0.0368) but not dying (P = 0.6126). Data were separated based on motor neuron position as in **(C)**. Graphs depict mean ± sem synapse number per micrometer of 66 ATF3+ and 61 cCasp3+ cells from five CS1–2 SOD^{G93A} mice (mean ± stdev age = 111 ± 2 postnatal days).

comprising the majority of motor neuron inhibitory input. Taken together, these data indicate that not only Renshaw cell but total V1 synaptic contacts onto motor neuron cell bodies increase on stressed and dying motor neurons in SOD^{G93A} mice, arguing against a premature loss of V1 synapses.

Fig. 4. Motor and inhibitory neuron loss along the rostro-caudal axis of spinal cord in control and SOD^{G93A} mice at late stages of disease. **(A, B)** Total motor neurons **(A)** and V1 inhibitory neurons **(B)** are decreased in CS5 SOD^{G93A} compared to control mice at brachial (C4–6), thoracic (T4–6) and lumbar (L3–5) spinal cord levels. Scatter dot plots represent average neuron number per 25 μm hemi-section as described in the legend to Fig. 1. P values < 0.001 for all comparisons. **(C)** Percentage loss of motor or V1 inhibitory neurons at brachial, thoracic or lumbar spinal cord levels at CS5. Scatter dot plots (top) or graph (bottom) of percent decrease in mean SOD^{G93A} v. CTL neuron number. Each dot represents a single litter-, age- and gender-matched pair. Graphs depict percent loss of brachial (blue), thoracic (green) and lumbar (red) total motor neurons (x-axis) versus V1 inhibitory neurons (y-axis). **(D–G)** Analysis of the V1 clades at brachial (C4–6), thoracic (T4–6) and lumbar (L3–5) levels in SOD^{G93A} versus control mice at CS5. V1^{FoxP2} inhibitory neurons **(D)** are similarly reduced in number at brachial (P = 0.003, 43% decrease), thoracic (P = 0.006, 39% decrease) and lumbar (P < 0.001, 49% decrease) levels. V1^{Sp8} inhibitory neurons **(E)** are reduced at brachial (P = 0.007, 38% decrease) and lumbar (P = 0.0087, 45% decrease) but not thoracic (P = 0.0919) levels. V1^{Pou6f2} **((F)**: brachial, P = 0.0915; thoracic, P = 0.2619; lumbar, P = 0.1975) and V1^{vCalbindin} **((G)**: brachial, P = 0.7732; thoracic, P = 0.2898; lumbar, P = 0.3603) inhibitory neurons are unaffected at all levels. Scatter dot plots represent average neuron number per 25 μm hemi-section as described in the legend to Fig. 1.

DISCUSSION

Increasing evidence suggests that deficits in motor output in ALS result not only from the initial loss of motor neurons but also from more widespread alteration of modulatory circuits that control their firing (van Zundert et al., 2012; King et al., 2016; Brownstone and Lancelin, 2018). Such alterations have not only been observed for spinal motor circuits, as we demonstrate here for the V1 inhibitory neuron class, but also for cortical motor circuits, in which compensatory changes and/or degeneration of cortical pre-motor subtypes occur (Zhang et al., 2016; Clark et al., 2017). Like motor neuron loss, these interneuron losses appear to be subtype-specific with certain classes, and even subpopulations within these classes, most affected—as we demonstrate here for the V1 clades and a clade-derived subpopulation. This growing evidence of selective, circuit-level changes raises several fundamental questions about the mechanisms that initiate and propagate ALS pathology, including what the origin is of ALS susceptibility, and whether a functional relationship exists between ALS-susceptible motor and interneuron subtypes in both the normal and diseased state.

Selective loss of spinal interneurons

We show here that subsets of spinal interneurons are lost in the SOD^{G93A} mouse model of ALS at late stages of disease. Our data support the idea that like motor neurons, V1 and V2a interneurons have an increased susceptibility compared to other interneuron classes. Approximately half of V1 inhibitory and a quarter of V2a excitatory neurons are preserved, even in the most affected animals, suggesting the existence of resistant interneuron subpopulations, akin to the gamma subclass of motor neurons. Examination of V1 inhibitory subpopulations lends further support to this idea, as V1 clades and clade-derived subsets vary further in their susceptibility. Such differences in susceptibility may derive from differences in the downstream molecular profiles, connectivity or function of individual V1 subpopulations. We cannot completely exclude however that sampling biases due to variant subpopulation size or rostro-caudal distribution could also contribute to different levels of susceptibility. Moreover, clades that are unaffected in cell number could exhibit subtle alterations in health or synaptic connectivity, not detected by our current analysis. Additionally, because V1 clades comprise only half of total V1 inhibitory neurons, how the other half may differ in ALS susceptibility remains an open question. These observed and potential differences in V1 susceptibility mirror those of motor neurons, raising the question of how the two might be causally related during disease progression in ALS.

Potential mechanisms of selective interneuron susceptibility

Our results also raise the question of what underlies the differences we observe in spinal interneuron susceptibility, across all interneuron types and within the V1 subclass. It is noteworthy that the loss of V2a excitatory neurons we observe mirrors the timing and severity of motor neuron loss at both early and late stages of disease progression in SOD ^{G93A} mice. The Chx10-expressing V2a excitatory neurons that we examine are known to make extensive direct synapses with motor neurons (Hayashi et al., 2018), and this direct connectivity could drive V2a loss either as a consequence of loss of their synaptic partners or through a trans-synaptic spreading of the disease, as has been previously been proposed for the focal spread of human ALS (Ravits, 2014). Such a ‘‘direct-connectivity” model would predict that neurons require their postsynaptic partner for survival during ALS progression. A more detailed time course analysis of markers of degeneration in connected neurons, with higher spatial and temporal resolution and in combination with genetic or viral ablation of one of the two interconnected subpopulations, could shed light on the potential for degenerative, trans-synaptic spread.

In contrast to the matching of V2a and motor neuron degeneration, the loss of V1 inhibitory neurons is less than that of motor neurons during disease progression. At both early and late stages, the relative magnitude of motor neuron loss is greater than that of V1 loss on average and even within the same SOD^{G93A} mouse. One potential explanation of this incongruence is that V1 inhibitory neurons, unlike V2a excitatory neurons, may have variant patterns of connectivity with motor neurons, such that some are directly connected whereas others influence motor neuron output through indirect, multi-synaptic connections, and thus are less affected. For example, the most susceptible V1^{FoxP2} subpopulation includes Ia-inhibitory interneurons that regulate flexor–extensor coordination by directly connecting to motor neurons of antagonist muscle pairs (Benito-Gonzalez and Alvarez, 2012). Alternatively, V1 susceptibility may derive from connections to susceptible motor neurons. For example, the resistance of V1^{Pou6f2} and thoracic V1^{Sp8} inhibitory neurons may stem from the fact that these connect only with ALS-resistant motor neuron types.

This model, however, is at odds with the relative resistance of the Renshaw cell, a V1 subpopulation making direct synaptic contact on ALS susceptible motor neurons. Our data indicate that the loss of Renshaw cells is less pronounced than other V1 subpopulations in later stage ALS animals, although a previous report found a marked reduction in this population at even more severe disease stages (Wootz et al., 2013). The delayed susceptibility of the Renshaw cell subpopulation, despite their known direct connectivity to susceptible motor neurons, may reflect the specific properties of this V1 class. Renshaw cells are unique in their morphology, connectivity and intrinsic physiological properties (Alvarez and Fyffe, 2007), and are the only V1 inhibitory neuron that both receives input from and synapses onto motor neurons. Renshaw cells additionally express abundant calcium binding proteins, including Calbindin and Parvalbumin, and use both GABA and glycine inhibitory neurotransmitters, properties that have been correlated with the resistance of neuronal subtypes in

the spinal cord, hindbrain and cortex (Alexianu et al., 1994; Appel et al., 2001; Lorenzo et al., 2006; Clark et al., 2017). Thus, the resistance of Renshaw cells may instead result from intrinsic resilience to disease-mediated degeneration.

This idea that intrinsic cellular properties might confer a greater susceptibility or resistance of some neuron classes compared to others also can be extended to the V1 clades, as they are by definition different in their transcriptional profiles. The consequences of these transcriptional signatures on cellular properties, while still largely unexplored, may include differences in neurotransmitter (GABA, Glycine, and GABA/Glycine), calcium binding proteins (Parvalbumin, Calbindin and Calretinin), or other intrinsic properties. On an anatomical level, V1 size and morphology could additionally vary between clades or differentially susceptible subpopulations and, on a physiological level, V1 inhibitory neurons at early postnatal stages exhibit markedly different active and passive membrane properties (Bikoff et al., 2016). Whether and how such intrinsic differences may contribute to selective susceptibility will become clearer as intrinsic properties are better defined for V1 clades under wildtype conditions. Our finding that the transcription factors that mark clades and clade-derived subtypes in early postnatal stages are conserved in their mutual exclusivity, cell body positioning, and relative numbers at adult stages lends some support to the idea that these subpopulations have different connectivity and functional properties that make them differentially susceptible to ALS.

V1 synaptic connectivity and ALS progression

Understanding how the changes we observe in spinal interneurons may influence motor neuron synaptic connectivity is crucial to unravel the role of motor circuits in ALS progression. Compensatory mechanisms to maintain circuit homeostasis have been proposed to explain the delay of any phenotypic symptoms of ALS until stages when greater than one third of motor neurons are lost. More specifically, such a compensatory mechanism has been suggested for Renshaw cells at the level of the synapse, wherein new Renshaw cell contacts onto motor neuron cell bodies appear at early stages of disease (Wootz et al., 2013). This finding suggests that inhibitory neurons at first may provide a protective effect by compensating for changes in motor neuron excitability and then, as they themselves degenerate, hasten disease progression and motor neuron loss—a model of circuit homeostasis (Brownstone and Lancelin, 2018).

Our analysis suggests that this homeostatic phenomenon is not restricted to Renshaw cells but may be a general feature of V1 inhibitory circuits, with total V1 synaptic contacts, both Calbindin-negative and Calbindin-positive, increasing on the cell bodies of stressed or dying motor neuron in SOD^{G93A} mice (Fig. 5). In fact, this increase in V1 synaptic number onto motor neuron cell bodies during disease progression is largely due to Calbindin-negative V1 inhibitory neurons, as they make up the bulk of direct inhibitory synapses in both a normal and diseased state. Several questions remain to be explored including whether this increase in cell body synaptic contacts occurs across the entire dendritic tree, whether it differs for each V1 clade, and how it may modulate motor neuron activity. Nonetheless, in a similar manner, an early increase in synaptic contacts has also been observed for the cholinergic V0c class (reviewed in Witts et al., 2014) and has yet to be explored for the excitatory V2a class, suggestive that modulation of synapse numbers occurs for other non-inhibitory neurons and raising the larger question of how the inhibitory-excitatory synaptic balance may be maintained or lost during ALS progression. Disruption of the inhibitory-excitatory synaptic balance at different disease stages and/or for different neuron types has the potential to contribute to the observed hypo or hyper-excitability phenotypes proposed to exacerbate ALS disease pathology (Van Den Bosch et al., 2006; de Martínez-Silva et al., 2018). A more detailed analysis of the inhibitory and excitatory circuits, and their relationship to motor neuron loss in ALS, is likely to be critical for understanding, and perhaps someday slowing, disease progression.

ACKNOWLEDGEMENTS

This work was made possible by the generous support of Project ALS. Imaging and related analyses were facilitated by The Waitt Advanced Biophotonics Center Core at the Salk Institute, supported by grants from NIH-NCI CCSG (P30 014195) and NINDS Neuroscience Center (NS072031). The authors would like to additionally thank Drs. Jane Dodd, Robert Brownstone, and Laskaro Zagoraiou for helpful comments on the manuscript. This manuscript is dedicated to Tom Jessell, an inspirational scientist, friend and mentor.

REFERENCES

Al-Chalabi A, Hardiman O (2013) The epidemiology of ALS: a conspiracy of genes, environment and time. Nat Rev Neurol 9:617–628.

Alexianu ME, Ho BK, Mohamed AH, La Bella V, Smith RG, Appel SH (1994) The role of calcium-binding proteins in selective motoneuron vulnerability in amyotrophic lateral sclerosis. Ann Neurol 36:846–858.

Alvarez FJ, Fyffe REW (2007) The continuing case for the Renshaw cell. J Physiol (Lond) 584:31–45.

Alvarez FJ, Jonas PC, Sapir T, Hartley R, Berrocal MC, Geiman EJ, Todd AJ, Goulding M (2005) Postnatal phenotype and localization of spinal cord V1 derived interneurons. J Comp Neurol 493:177–192.

Appel SH, Beers D, Siklos L, Engelhardt JI, Mosier DR (2001) Calcium: the Darth Vader of ALS. Amyotroph Lateral Scler Other Motor Neuron Disord 2(Suppl 1):S47–S54.

Benito-Gonzalez A, Alvarez FJ (2012) Renshaw cells and Ia inhibitory interneurons are generated at different times from p1 progenitors and differentiate shortly after exiting the cell cycle. J Neurosci 32:1156–1170.

Bikoff JB, Gabitto MI, Rivard AF, Drobac E, Machado TA, Miri A, Brenner-Morton S, Famojure E, Diaz C, Alvarez FJ, Mentis GZ, Jessell TM (2016) Spinal inhibitory interneuron diversity delineates variant motor microcircuits. Cell 165:207–219.

Brownstone RM, Lancelin C (2018) Escape from homeostasis: spinal microcircuits and progression of amyotrophic lateral sclerosis. J Neurophysiol 119:1782–1794.
Carr PA, Alvarez FJ, Leman EA, Fyffe RE (1998) Calbindin D28k expression in immunohistochemically identified Renshaw cells. Neuroreport 9:2657–2661.
Chang Q, Martin LJ (2009) Glycinergic innervation of motoneurons is deficient in amyotrophic lateral sclerosis mice: a quantitative confocal analysis. Am J Pathol 174:574–585.
Chiu AY, Zhai P, Dal Canto MC, Peters TM, Kwon YW, Prattis SM, Gurney ME (1995) Age-dependent penetrance of disease in a transgenic mouse model of familial amyotrophic lateral sclerosis. Mol Cell Neurosci 6:349–362.
Clark RM, Blizzard CA, Young KM, King AE, Dickson TC (2017) Calretinin and Neuropeptide Y interneurons are differentially altered in the motor cortex of the SOD1G93A mouse model of ALS. Sci Rep 7:44461–44513.
Crone SA, Quinlan KA, Zagoraiou L, Droho S, Restrepo CE, Lundfald L, Endo T, Setlak J, Jessell TM, Kiehn O, Sharma K (2008) Genetic ablation of V2a ipsilateral interneurons disrupts left-right locomotor coordination in mammalian spinal cord. Neuron 60:70–83.
Dasen JS, Jessell TM (2009) Hox networks and the origins of motor neuron diversity. Curr Top Dev Biol 88:169–200.
Ericson J, Rashbass P, Schedl A, Brenner-Morton S, Kawakami A, van Heyningen V, Jessell TM, Briscoe J (1997) Pax6 controls progenitor cell identity and neuronal fate in response to graded Shh signaling. Cell 90:169–180.
Fischer LR, Culver DG, Tennant P, Davis AA, Wang M, Castellano-Sanchez A, Khan J, Polak MA, Glass JD (2004) Amyotrophic lateral sclerosis is a distal axonopathy: evidence in mice and man. Exp Neurol 185:232–240.
Francius C, Harris A, Rucchin V, Hendricks TJ, Stam FJ, Barber M, Kurek D, Grosveld FG, Pierani A, Goulding M, Clotman F (2013) Identification of multiple subsets of ventral interneurons and differential distribution along the rostrocaudal axis of the developing spinal cord Winkler C, ed.. PLoS ONE 8:e70325.
Frey D, Schneider C, Xu L, Borg J, Spooren W, Caroni P (2000) Early and selective loss of neuromuscular synapse subtypes with low sprouting competence in motoneuron diseases. J Neurosci 20:2534–2542.
Gabitto MI, Pakman A, Bikoff JB, Abbott LF, Jessell TM, Paninski L (2016) Bayesian sparse regression analysis documents the diversity of spinal inhibitory interneurons. Cell 165:220–233.
Gosgnach S, Bikoff JB, Dougherty KJ, Manira El A, Lanuza GM, Zhang Y (2017) Delineating the diversity of spinal interneurons in locomotor circuits. J Neurosci 37:10835–10841.
Gurney ME, Pu H, Chiu AY, Dal Canto MC, Polchow CY, Alexander DD, Caliendo J, Hentati A, Kwon YW, Deng HX (1994) Motor neuron degeneration in mice that express a human Cu, Zn superoxide dismutase mutation. Science 264:1772–1775.
Hardiman O, Al-Chalabi A, Chio A, Corr EM, Logroscino G, Robberecht W, Shaw PJ, Simmons Z, van den Berg LH (2017) Amyotrophic lateral sclerosis. Nat Rev Dis Primers 3:17085–17091.
Hayashi M, Hinckley CA, Driscoll SP, Moore NJ, Levine AJ, Hilde KL, Sharma K, Pfaff SL (2018) Graded Arrays of spinal and supraspinal V2a interneuron subtypes underlie forelimb and hindlimb motor control. Neuron 97. 869.e5–884.e5.
Herron LR, Miles GB (2012) Gender-specific perturbations in modulatory inputs to motoneurons in a mouse model of amyotrophic lateral sclerosis. Neuroscience 226:313–323.
Hossaini M, Cardona Cano S, van Dis V, Haasdijk ED, Hoogenraad CC, Holstege JC, Jaarsma D (2011) Spinal inhibitory interneuron pathology follows motor neuron degeneration independent of glial mutant superoxide dismutase 1 expression in SOD1-ALS mice. J Neuropathol Exp Neurol 70:662–677.
Kanning KC, Kaplan A, Henderson CE (2010) Motor neuron diversity in development and disease. Annu Rev Neurosci 33:409–440.
Kaplan A, Spiller KJ, Towne C, Kanning KC, Choe GT, Geber A, Akay T, Aebischer P, Henderson CE (2014) Neuronal matrix metalloproteinase-9 is a determinant of selective neurodegeneration. Neuron 81:333–348.
Kaur SJ, McKeown SR, Rashid S (2016) Mutant SOD1 mediated pathogenesis of amyotrophic lateral sclerosis. Gene 577:109–118.
King AE, Woodhouse A, Kirkcaldie MTK, Vickers JC (2016) Excitotoxicity in ALS: overstimulation, or overreaction? Exp Neurol 275(Pt 1):162–171.
Konsolaki E, Koropouli E, Pothakos K, Zagoraiou L, submitted for consideration in this issue. Neuroscience.
Lorenzo L-E, Barbe A, Portalier P, Fritschy J-M, Bras H (2006) Differential expression of GABAA and glycine receptors in ALS-resistant vs. ALS-vulnerable motoneurons: possible implications for selective vulnerability of motoneurons. Eur J Neurosci 23:3161–3170.
Lalancette-Hébert M, Sharma A, Lyashchenko AK, Shneider NA (2016) Gamma motor neurons survive and exacerbate alpha motor neuron degeneration in ALS. Proc Natl Acad Sci USA 113: E8316–E8325.
Landoni LM, Myles JR, Wells TL, Mayer WP, Akay T (2019) Cholinergic modulation of motor neurons through the C-boutons are necessary for the locomotor compensation for severe motor neuron loss during amyotrophic lateral sclerosis disease progression. Behav Brain Res 369 111914.
Li M, Ona VO, Guégan C, Chen M, Jackson-Lewis V, Andrews LJ, Olszewski AJ, Stieg PE, Lee JP, Przedborski S, Friedlander RM (2000) Functional role of caspase-1 and caspase-3 in an ALS transgenic mouse model. Science 288:335–339.
Lutz C (2018) Mouse models of ALS: Past, present and future. Brain Res 1693:1–10.
Madisen L, Zwingman TA, Sunkin SM, Oh SW, Zariwala HA, Gu H, Ng LL, Palmiter RD, Hawrylycz MJ, Jones AR, Lein ES, Zeng H (2010) A robust and high-throughput Cre reporting and characterization system for the whole mouse brain. Nat Neurosci 13:133–140.
Martínez-Silva M de L, Imhoff-Manuel RD, Sharma A, Heckman CJ, Shneider NA, Roselli F, Zytnicki D, Manuel M (2018) Hypoexcitability precedes denervation in the large fast-contracting motor units in two unrelated mouse models of ALS. Elife 7:1958.
Morisaki Y, Niikura M, Watanabe M, Onishi K, Tanabe S, Moriwaki Y, Okuda T, Ohara S, Murayama S, Takao M, Uchida S, Yamanaka K, Misawa H (2016) Selective expression of osteopontin in ALS-resistant motor neurons is a critical determinant of late phase neurodegeneration mediated by matrix metalloproteinase-9. Sci Rep 6:27354.
Pasinelli P, Houseweart MK, Brown RH, Cleveland DW (2000) Caspase-1 and -3 are sequentially activated in motor neuron death in Cu, Zn superoxide dismutase-mediated familial amyotrophic lateral sclerosis. Proc Natl Acad Sci USA 97:13901–13906.
Pullen AH, Athanasiou D (2009) Increase in presynaptic territory of C-terminals on lumbar motoneurons of G93A SOD1 mice during disease progression. Eur J Neurosci 29:551–561.
Pun S, Santos AF, Saxena S, Xu L, Caroni P (2006) Selective vulnerability and pruning of phasic motoneuron axons in motoneuron disease alleviated by CNTF. Nat Neurosci 9:408–419.
Ravits J (2014) Focality, stochasticity and neuroanatomic propagation in ALS pathogenesis. Exp Neurol 262 Pt B:121–126.
Romer SH, Seedle K, Turner SM, Li J, Baccei ML, Crone SA (2017) Accessory respiratory muscles enhance ventilation in ALS model mice and are activated by excitatory V2a neurons. Exp Neurol 287:192–204.
Sapir T, Geiman EJ, Wang Z, Velasquez T, Mitsui S, Yoshihara Y, Frank E, Alvarez FJ, Goulding M (2004) Pax6 and engrailed 1 regulate two distinct aspects of renshaw cell development. J Neurosci 24:1255–1264.
Solomon JA, Tarnopolsky MA, Hamadeh MJ (2011) One universal common endpoint in mouse models of amyotrophic lateral sclerosis. Dawson TM, ed.. PLoS ONE 6:e20582.

Stephens B, Guiloff RJ, Navarrete R, Newman P, Nikhar N, Lewis P (2006) Widespread loss of neuronal populations in the spinal ventral horn in sporadic motor neuron disease. A morphometric study. J Neurol Sci 244:41–58.

Sweeney LB, Bikoff JB, Gabitto MI, Brenner-Morton S, Baek M, Yang JH, Tabak EG, Dasen JS, Kintner CR, Jessell TM (2018) Origin and segmental diversity of spinal inhibitory interneurons. Neuron 97:341–355.e343.

Van Den Bosch L, Van Damme P, Bogaert E, Robberecht W (2006) The role of excitotoxicity in the pathogenesis of amyotrophic lateral sclerosis. Biochim Biophys Acta 1762:1068–1082.

van Zundert B, Izaurieta P, Fritz E, Alvarez FJ (2012) Early pathogenesis in the adult-onset neurodegenerative disease amyotrophic lateral sclerosis. J Cell Biochem 113:3301–3312.

Wetts R, Vaughn JE (1996) Differential vulnerability of two subsets of spinal motor neurons in amyotrophic lateral sclerosis. Exp Neurol 141:248–255.

Witts EC, Zagoraiou L, Miles GB (2014) Anatomy and function of cholinergic C bouton inputs to motor neurons. J Anat 224:52–60.

Wootz H, Fitzsimons-Kantamneni E, Larhammar M, Rotterman TM, Enjin A, Patra K, André E, van Zundert B, Kullander K, Alvarez FJ (2013) Alterations in the motor neuron-renshaw cell circuit in the Sod 1(G93A) mouse model. J Comp Neurol 521:1449–1469.

Zhang J, Lanuza GM, Britz O, Wang Z, Siembab VC, Zhang Y, Velasquez T, Alvarez FJ, Frank E, Goulding M (2014) V1 and v2b interneurons secure the alternating flexor-extensor motor activity mice require for limbed locomotion. Neuron 82:138–150.

Zhang W, Zhang L, Liang B, Schroeder D, Zhang Z-W, Cox GA, Li Y, Lin D-T (2016) Hyperactive somatostatin interneurons contribute to excitotoxicity in neurodegenerative disorders. Nat Neurosci 19:557–559.

APPENDIX A. SUPPLEMENTARY DATA

Supplementary data to this article can be found online at https://doi.org/10.1016/j.neuroscience.2020.08.011.

(Received 18 February 2020, Accepted 7 August 2020)
(Available online 25 August 2020)